

1 **Title:** Physiological basis of noise-induced hearing loss in a tympanal ear

2 **Abbreviated title:** Hearing loss in an insect ear

3 **Authors** (corresponding with *): Ben Warren^{1*}, Georgina E Fenton^{1,2}, Elizabeth Klensch³, James
4 FC Windmill³, Andrew S French⁴

5 **Author Affiliations:** 1 Department of Neuroscience, Psychology and Behaviour, University of
6 Leicester, Leicester, LE1 7RH, UK **Corresponding author: Ben Warren, bw120@le.ac.uk**

7 2 Current address: Center of Advanced European Studies and Research, Stiftung Caesar Ludwig-
8 Erhard-Allee 2, D-53175, Bonn, Nordrhein-Westfalen, Germany

9 3 Centre for Ultrasonic Engineering, Department of Electronic and Electrical Engineering, University
10 of Strathclyde, 204 George Street, Glasgow, G1 1XW, UK

11 4 Department of Physiology and Biophysics, Dalhousie University, PO Box 15000, Halifax, Nova
12 Scotia, B3H 4R2, Canada

13 **Number of pages:** 29 **Number of figures and tables:** 7 Figures, 1 Table **Number of words:**
14 Abstract 159, Introduction 650, Discussion 1492

15 **Abstract**

16 Acoustic overexposure, such as listening to loud music too often, results in noise-induced hearing
17 loss. The pathologies of this prevalent sensory disorder begin within the ear at synapses of the
18 primary auditory receptors, their postsynaptic partners and their supporting cells. The extent of
19 noise-induced damage, however, is determined by over-stimulation of primary auditory receptors,
20 upstream of where the pathologies manifest. A systematic characterisation of the
21 electrophysiological function of the upstream primary auditory receptors is warranted to understand
22 how noise-exposure impacts on downstream targets, where the pathologies of hearing loss begin.
23 Here, we used the experimentally-accessible locust ear (male, *Schistocerca gregaria*) to
24 characterise a decrease in the auditory receptor's ability to respond to sound after noise exposure.
25 Surprisingly, after noise exposure, the electrophysiological properties auditory receptors remains
26 unchanged, despite a decrease in the ability to transduce sound. This auditory deficit stems from
27 changes in a specialised receptor lymph that bathes the auditory receptors – revealing striking
28 parallels with the mammalian auditory system.

29 **Significance Statement**

30 Noise exposure is the largest preventable cause of hearing loss. It is the auditory receptors that bear
31 the initial brunt of excessive acoustic stimulation, because they must convert excessive sound-
32 induced movements into electrical signals, but remain functional afterward. Here we use the
33 accessible ear of an invertebrate to – for the first time in any animal - characterise changes in
34 auditory receptors after noise overexposure. We find that their decreased ability to transduce sound
35 into electrical signals is, most probably, due to changes in supporting (scolopale) cells that maintain
36 the ionic composition of the ear. An emerging doctrine in hearing research is that vertebrate primary
37 auditory receptors are surprisingly robust, something which we show rings true for invertebrate ears
38 too.

39

40 **Competing Interests:** The authors declare no competing financial interests.

41 **Acknowledgements**

42 BW was funded by the Royal Society and the Leverhulme Trust. Within the University of Leicester
43 BW was also funded by the Department of Neuroscience, Psychology and Behaviour and the
44 Wellcome Trust Institutional Strategic Support Fund. GF was funded by a Royal Society

45 Enhancement Award. Work carried out by EK and JFCW was funded by the European Research
46 Council under the European Union's Seventh Framework Programme (FP/2007-2013) / ERC Grant
47 Agreement n. 615030. Andrew French is funded by Discovery Grant RGPIN/03712 from the Natural
48 Sciences and Engineering Research Council of Canada. We would also like to thank Neil Rimmer
49 and Jake Cranston for locust husbandry and Ben Cooper and Brendan O'Connor for help with
50 statistical analysis and making sure the locust treatment remained blinded to the experimenter. I
51 would also like to thank Nathan Suray for performing preliminary experiments for *in vivo* hook
52 electrode recordings.

53

54 **Introduction: Consequences of noise-induced hearing loss across animal ears**

55 Our senses endow us with an incredible subjective experience of our world. The gatekeepers of this external
56 sensory environment – sensory receptors – selectively encode stimuli into electrical signals to give us our
57 five senses. Overstimulation of sensory neurons, however, leads to damage and the sound-sensitive cells in
58 our ears are particularly prone to permanent injury (Lundström & Johansson, 1986; Young, 1988; Salvi &
59 Boettcher, 2008). As a result, the most common sensory impairment in humans is hearing loss and the
60 majority of preventable hearing loss is due to excessive noise exposure.

61 The ears of all animals have specialised ciliated sound-sensitive receptor cells, likely of a common
62 evolutionary origin (Fritzsche & Beisel, 2004), that transduce sound into electrical potentials. Critical to this
63 process of auditory transduction are stretch-sensitive ion channels, embedded in the membranes of the cilia,
64 which open in response to sound (Gillespie & Walker, 2001; Albert & Kozlov, 2016). Common to arthropod
65 hearing is the maintenance of a specialised cation-rich lymph, by supporting cells, which bathe the cilia of
66 auditory receptor cells. In insects, a single supporting scolopale cell encloses the cilium and pumps cations
67 into the receptor lymph. Similarly, in the cochlea of mammals (in the stria vascularis) three groups of
68 supporting cells pump cations into the endolymph. This generates a high electrochemical gradient such that
69 when the transduction ion channels are opened by sound cations flow into the auditory receptor cells to
70 generate the primary electrical signal – the receptor potential. In Orthoptera, such as locusts and crickets,
71 the transduction potential is converted into a small dendritic spike that travels along a single dendrite of the
72 neuron (Hill, 1983b; Oldfield & Hill, 1986) to the soma. There, most probably in the axon hillock, it triggers a
73 larger axonal spike, at its basal end, that carries auditory information to the central nervous system (Warren
74 & Matheson, 2018).

75 Two decades ago, it was assumed that the pathologies of hearing loss (such as spiral ganglion neuron loss)
76 result from, and after, a loss of 'upstream' hair cells (Bohne and Harding, 2000). A decade ago this doctrine
77 was challenged as noise exposure was found to reduce hearing thresholds without any loss of hair cells
78 (Kujawa and Liberman, 2009; Lin et al., 2011). Hair cells, therefore, appear more resilient than first thought
79 and are not necessarily the primary source of hearing loss. None-the-less, in response to loud noise, the
80 primary auditory receptors of any animal will experience an excessive influx of cations. This influx leads to
81 production of reactive oxygen species by mitochondria (Yamane et al., 1995), damage of mitochondria
82 (Christie et al., 2003) and glutamatergic excitotoxicity (Kujawa & Liberman, 2009; Pujol et al., 1993), which
83 can trigger apoptotic and necrotic pathways (Wagner & Shin, 2019). A recurring target of damage in auditory
84 systems is in the supporting cells (Shi et al., 2015; Yamashita et al., Yamane et al., 1995; Yamasoba et al.,
85 1998) which, when damaged or genetically altered, fail to pump a normal amount of cations into the receptor
86 lymph that bathes the cilia of the primary auditory receptors (Hirose & Liberman, 2003; Li et al., 1997; Ma et
87 al., 1995; Vassout, 1984), which can lead to auditory pathologies (Christie & Eberl, 2014; Roy et al., 2013).

88 Despite the severe effects of noise in auditory systems, there is no systematic understanding of changes in
89 the electrophysiological properties and function of the auditory receptor cells themselves shortly after noise
90 exposure for any animal. The locust ear permits a detailed characterisation of the sound-elicited ionic currents
91 because whole-cell patch-clamp recordings can be conducted during concurrent stimulation by airborne
92 sound in an intact ear (Warren and Matheson, 2018) - an approach not possible in other hearing models. In
93 response to acoustic overstimulation we measured physiological changes in the sound-evoked
94 displacements of the tympanum, electrical responses from the auditory nerve, ionic currents in individual
95 auditory neurons, and relative abundances of some putative sound-activated ion channel genes.

96

97 **Materials and methods**

98 *Locust husbandry*

99 Desert locusts (*Schistocerca gregaria*) were reared in crowded conditions (phase gregaria) on a 12:12 h
100 light:dark cycle at 36:25°C. Locusts were fed on a combination of fresh wheat and bran *ab libitum*. Male
101 locusts between 10 and 20 days post imaginal moult were used for all experiments. We used new locusts for
102 each set of experiments. We are willing and open to share our locust strains with other research groups.

103 *Noise exposure and acoustic stimulation*

104 The wings of all locusts were cut off at their base to increase noise exposure of the conditioning tone to their
105 tympanal ears, which are otherwise covered by their wings. Up to twenty locusts, for both the noise-exposed
106 group and the control group, were placed in a cylindrical wire mesh cage (8 cm diameter, 11 cm height). Both
107 cages were placed directly under a speaker (Visaton FR 10 HM 4 OHM, RS Components Ltd). For the noise-
108 exposed group only, the speaker was driven by a function generator (Thurlby Thandar Instruments TG550,
109 RS Components Ltd) and a sound amplifier (Monacor PA-702, Insight Direct Ltd) to produce a 3 kHz tone at
110 126 dB SPL, measured at the top of the cage where locusts tended to accumulate. This tone was played
111 continuously for 24 hours for the noise-exposed group. The control group was housed in an identical cage
112 with a silent speaker for 24 hours. All mechanical and electrophysiological recordings were performed within
113 eight hours of cessation of noise-exposure. Sound Pressure Levels (SPLs) were measured with a
114 microphone (Pre-03 Audiomatica, DBS Audio) and amplifier (Clio Pre 01 preamp, DBS Audio). The
115 microphone was calibrated with a B&K Sound Level Calibrator (CAL73, Mouser Electronics). The locust ear
116 was stimulated with the same speaker and amplifier as above for hook electrode recordings at 3 kHz with a
117 rise and fall time of 2 ms. For intracellular recordings from individual auditory neurons the speaker was driven
118 by a custom made amplifier controlled by a EPC10-USB patch-clamp amplifier (HEKA-Elektronik) controlled
119 by the program Patchmaster (version 2x90.2, HEKA-Elektronik) running under Microsoft Windows (version
120 7).

121 *Biomechanical measurements of the tympanum with laser Doppler vibrometry*

122 For *in vivo* measurements the locusts wings and hind legs were cut off and locusts were fixed so that their
123 tympanum was perpendicular to the micro-scanning Laser Doppler Vibrometer (PSV 300, Polytec,
124 Waldbronn, Germany) with a close up unit (OFV 056). A loudspeaker (ESS Air Motion Transformer, South El
125 Monte, CA, USA) was placed at least 10 cm away, to avoid operating in the near field. A microphone (Brüel
126 & Kjær 4138, Naerum, Denmark) was positioned to measure the sound pressure at the tympanal membrane.

127 For *ex vivo* measurements whole ears, including Müller's Organ attached to the internal side of the
128 tympanum, were dissected from the first abdominal segment, by cutting around the small rim of cuticle
129 surrounding the tympanum with a fine razor blade. Trachea and the auditory nerve (Nerve 6) were cut with
130 fine scissors (5200-00, Fine Science Tools), and the trachea and connective tissue removed with fine forceps.

131 The ear was secured, inner side up, into a 2 mm diameter hole in a Perspex divider (go to
132 www2.le.ac.uk/departments/npb/people/bw120 to download the locust ear holder file for 3D printing) using
133 an insect pin pushed through the anterior rim of cuticle and into 2 mm of Sylgard (184 Silicone Elastomer,
134 Dow Corning) on the base of a 30 mm diameter petri dish. The tympanum in its holder was positioned at an
135 angle of 30° off vertical to observe Group-III neurons of Müller's Organ from above. A watertight seal was
136 made between the ear cuticle and the divider hole with dental glue (Protemp 4, 3M ESPE) and nerve 6 was
137 secured into the glue at the ventral border of the tympanum.

138 *In vivo hook electrode recordings from auditory nerve six*

139 Locusts were secured ventral side up in plasticine. A section of the second and third ventral thoracic segment
140 was cut with a fine razor blade and removed with fine forceps. Tracheal air sacks were removed to expose
141 nerve six and the metathoracic ganglia. Hook electrodes constructed from silver wire 18 µm diameter
142 (AG549311, Advent Research Materials Ltd) were hooked under the nerve and the nerve was lifted out of
143 the haemolymph. Signals were amplified 10,000 times by a differential amplifier (Neurolog System) then
144 filtered with a 500 Hz high pass filter and a 50 kHz low pass filter. This amplified and filtered data was sampled
145 at 25 kHz by Spike2 (version 8) software running on Windows (version 10). To count the number of nerve
146 potentials for hook electrode recordings we counted each potential above 50 µV. We did this for all locusts
147 irrespective of the treatment of the locust for an objective measure of hearing function and all locusts were
148 used for analysis. N.B. the locust treatment was blinded to the experimenter until all data was collected and
149 analysed. For measurements of tone-evoked spike latency we only measured latencies where there was a
150 clear tone-elicited nerve potential above 50 µV. Thresholds were determined as the minimum SPL necessary
151 to get an increase in the nerve response. An increase in the nerve response, or threshold, was classified
152 when the nerve potential count is sequentially higher for each of the next three highest SPL tones (i.e. the
153 threshold was 40 dB SPL when the number of nerve potentials was higher at 50 dB SPL, then higher again
154 for 60 dB SPL, and higher still for 70 dB SPL).

155 *Dissection of Müller's Organ and isolation of Group-III auditory neurons and discovery of a muscle through*
156 *which the nerve of Müller's organ loops*

157 We focused our analyses on group-III auditory neurons because they form the majority of auditory neurons
158 of the Müller's organ (~46 out of ~80) (Jacobs et al., 1999), they are the most sensitive auditory neurons of

159 the Müller's organ (Römer, 1976) and whole-cell patch-clamp recordings were only possible from these
160 neurons (Warren and Matheson, 2018). For intracellular patch-clamp recordings from individual auditory
161 neurons the abdominal ear was excised and placed into a preparation dish as explained above
162 (*Biomechanical measurements of the tympanum with laser Doppler vibrometry*). This preparation allowed
163 perfusion of saline to the internal side of the tympanum, necessary for water-immersion optics for visualizing
164 Müller's Organ and the auditory neurons to be patch-clamped, and concurrent acoustic stimulation to the dry
165 external side of the tympanum. The inside of the tympanum including Müller's Organ was constantly perfused
166 in extracellular saline.

167 To expose Group-III auditory neurons for patch-clamp recordings, a solution of collagenase (0.5 mg/ml) and
168 hyaluronidase (0.5 mg/ml) (C5138, H2126, Sigma Aldrich) in extracellular saline was applied onto the medial-
169 dorsal border of Müller's Organ through a wide (12 μ m) patch pipette to digest the capsule enclosing Müller's
170 Organ and the Schwann cells surrounding the auditory neurons. Gentle suction was used through the same
171 pipette to remove the softened material and expose the membrane of Group-III auditory neurons. The somata
172 were visualized with an upright microscope (BH-2, Olympus) using a water immersion objective (W Plan-
173 APOCHROMAT, 40x, 1.0 numerical aperture, 2.5 mm working distance, Zeiss) and differential interference
174 contrast optics.

175 The auditory nerve of the Müller's organ passes through a striated muscle that is anchored on the lateral side
176 of the tympanic rim, near a spiracle opening. We hypothesise that this muscle could contract, pulling the
177 Müller's organ nerve and tympanum taught, in response to loud noise to prevent excessive sound induced
178 vibrations.

179 *Electrophysiological recordings and isolation of the transduction current*

180 In order to quantitatively record tone-evoked currents and spikes from individual auditory neurons the ear
181 was excised from the locust, and Müller's organ was immersed in saline. This is necessary to gain access
182 to, image and record from individual auditory neurons through whole-cell patch-clamp intracellular recordings
183 (Warren & Matheson, 2018). Electrodes with tip resistances between 3 and 4 M Ω were fashioned from
184 borosilicate glass (0.86 mm inner diameter, 1.5 mm outer diameter; GB150-8P, Science Products GmbH)
185 with a vertical pipette puller (PP-830, Narishige). Recording pipettes were filled with intracellular saline
186 containing the following (in mM): 190 K-aspartate, 4 NaCl, 2 MgCl₂, 1 CaCl₂, 10 HEPES, 10 EGTA. To block

187 K⁺ channels necessary for isolation the transduction current 20 mM tetraethylammonium chloride (TEA) was
188 added to the intracellular saline, K-aspartate was reduced to 170 mM to maintain the same osmolality. To
189 isolate the transduction current we also blocked spikes with 90 nM Tetrodotoxin (TTX) in the extracellular
190 saline. During experiments, Müller's Organs were perfused constantly with extracellular saline containing the
191 following in mM: 185 NaCl, 10 KCl, 2 MgCl₂, 2 CaCl₂, 10 HEPES, 10 Trehalose, 10 Glucose. The saline was
192 adjusted to pH 7.2 using NaOH. The osmolality of the intracellular and extracellular salines' were 417 and
193 432 mOsm, respectively.

194 Dihydrostreptomycin sesquisulfate, 50 μM (D7253, Sigma Aldrich) was used to block mechanotransduction
195 ion channels. Dihydrostreptomycin sesquisulfate was perfused at least 15 min before recordings. Whole-cell
196 voltage-clamp recordings were performed with an EPC10-USB patch-clamp amplifier (HEKA-Elektronik)
197 controlled by the program Patchmaster (version 2x90.2, HEKA-Elektronik) running under Microsoft Windows
198 (version 7). Electrophysiological data were sampled at 50 kHz. Voltage-clamp recordings were low-pass
199 filtered at 2.9 kHz with a four-pole Bessel filter. Compensation of the offset potential were performed using
200 the "automatic mode" of the EPC10 amplifier and the capacitive current was compensated manually. The
201 calculated liquid junction potential between the intracellular and extracellular solutions was also compensated
202 (15.6 mV for normal saline and 13.5 mV for TTX and TEA saline; calculated with Patcher's-PowerTools plug-
203 in from www3.mpibpc.mpg.de/groups/neher/index.php?page=software). Series resistance was
204 compensated between 50 and 70% with a time constant of 100 μs.

205 *Staining and confocal microscopy*

206 To stain Group-III auditory neurons, recording electrodes were filled with Neurobiotin (1% m/v, SP-1120,
207 Vector Laboratories) dissolved in intracellular saline. To aid diffusion of Neurobiotin into the neurons a
208 positive current of ~200 pA was injected for ~30 min. Directly after staining, Müller's Organs were fixed
209 overnight at 5°C in 4% paraformaldehyde (P6148, Sigma Aldrich) dissolved in Phosphate Buffer Saline
210 (PBS). Müller's Organs were then washed three times in PBS then gently shaken at room temperature for 20
211 min in a mixture of collagenase (0.5 mg/ml) and hyaluronidase (0.5 mg/ml) (C5138 and H2126, Sigma
212 Aldrich). They were washed three times in PBS (3x10 min) then gently shaken at room temperature in 0.2 %
213 m/v Triton-X100 dissolved in PBS (2x60 min). Müller's Organs were then gently shaken in 20 μg/ml Dylight
214 488 strepavidin (SA-5488, Vector Laboratories) and 0.05 mg/ml DAPI (D9542, Sigma Aldrich) in PBS

215 overnight at 5°C. During this time the fluorescent streptavidin binds very tightly to the fixed neurobiotin to
216 specifically stain the recorded neurons. After this overnight incubation the Müller's organs were washed three
217 times in PBS (3x10 min), dehydrated in an ethanol series and cleared in Methyl salicylate (M6752, Sigma
218 Aldrich).

219 Fluorescence images (pixel size 0.31 μm^2 , z stacks of 0.31 μm) were captured with a confocal microscope
220 (FV1000 CLSM, Olympus) equipped with Plan-UPlanSApo 10x (0.4 numerical aperture) and 20x (0.75
221 numerical aperture) lenses. Fluorescence emission of Dylight 488 was collected through a 505-530 nm
222 bandpass filter. Confocal images were adjusted for contrast and brightness, overlaid and stacked in ImageJ
223 (version 1.51, National Institutes of Health). The ImageJ plugin Simpler Neurite Tracer was used to determine
224 the distance from the centre of the soma to the dendrite dilation (Fig. 3C).

225 *RNA extraction, sequencing and transcriptome analysis*

226 A total of 320 Müller's organs from 160 control locusts (two ears per locust) and 320 Müller's organs from
227 160 noise-exposed locusts were extracted by grasping the Müller's organ through the tympanum with fine
228 forceps and pulling it out. Müller's organ RNA extraction took place within four hours after the 24 hr noise-
229 exposure was finished. Müller's organs were placed in an Eppendorf tube submerged in liquid nitrogen. RNA
230 was extracted and then treated with DNase using a Thermo-fisher RNAqueous kit (AM1931, ThermoFisher).
231 RNA was shipped in dry ice to Beijing Genomics Institute (Hong Kong) for sequencing. The samples were
232 quality checked and had RNA Integrity Values (RIN) of 8.7 and 8.4 for control and noise-exposed samples,
233 respectively. The two samples were sequenced using Illumina HiSeq 2000 using a 100 paired ends module.
234 We obtained 186.1 million clean reads for RNA extracted from the Müller's organs of noise-exposed locusts
235 and 185.9 million clean reads from the Müller's organs of control locusts. We analysed the RNA reads and
236 quantified expression levels (abundances) for the three genes that compose the two mechanotransduction
237 ion channel candidates in insects: *nompC*, *nanchung* and *inactive* (*nanchung* and *inactive* together code a
238 single heteromeric Nanchung-Inactive ion channel) and the two housekeeping genes *actin* and *GAPDH*.
239 Initial cDNA reads were groomed to have 80 or more contiguous nucleotides with Phred score >19 to give a
240 final database of ~100 million pairs of reads. Sequences of interest were identified by searching all possible
241 translations of reads from the control transcriptome versus amino acid sequences of published insect genes,
242 including *Drosophila melanogaster*, using BLOSUM matching matrices (Henikoff & Henikoff, 1993). Identified

243 reads of interest were extended by the transcriptome walking algorithm (French, 2012) using an initial
244 minimum overlap of 60 nucleotides. Walking was always continued to identify the complete protein coding
245 sequence, including both START and STOP codons.

246 Relative abundances of transcribed mRNA sequences in the two tissues were estimated by searching each
247 complete groomed transcriptome library for reads matching the reading frame of each gene, using the
248 criterion of at least 90/100 identical nucleotide matches to score each read as derived from the gene.
249 Matching reads as a fraction of total reads counted were then normalized by gene length and expressed as
250 abundance relative to the most abundant *actin* gene in the control tissue.

251 *Experimental design and statistical analysis*

252 For all recordings we used male *Schistocerca gregaria* from the Leicester 'Locust Labs' laboratory stock.
253 Throughout the manuscript n refers to the number of recorded neurons and N refers to the number of Müller's
254 Organ preparations used to achieve these recordings (i.e. n=10, N=6 means that 10 neurons were recorded
255 from 6 Müller's Organs). All n numbers are displayed on the figures for clarity. The reason for variation in n
256 numbers for some figures (e.g. Fig 4D) is because noise-exposed auditory neurons failed to produce a
257 response at lower SPLs compared to auditory neurons from control locusts. The Spread of the data is
258 indicated by 1 standard deviation as the standard deviation indicates the spread of the data, unlike standard
259 error. Median and Q1 and Q3 are displayed by bars when individual measurements are plotted. The treatment
260 of the locust: noise-exposed or control, remained blinded to the experimenter until data analysis was
261 completed. To test for differences and interactions between control, noise-exposed and streptomycin-treated
262 locusts we used either a linear model (LM) or Linear Mixed Effects Model (LMEM), with dB SPL and treatment
263 as fixed effects, and Locust ID as a random intercept, when repeated measured are reported. We used a
264 Wilcoxon test when comparing thresholds of hearing for hook electrode recordings (Fig. 2E, inset), as this
265 data was not continuous. Models were fitted in R (Version 3.4.3) with the package LME4 (Bates et al., 2015).
266 The test statistic for these analyses (t) are reported with the degrees of freedom (in subscript) and p value,
267 which are approximated using Satterthwaite equation (lmerTest package) (Kuznetsova et al., 2017). We
268 report Cohen's d effect size for significant differences. Curves where fitted to the data using Matlab (version
269 R2018a). The shape of the data was described by fitting Boltzmann voltage equation using non-linear least
270 squares method. For each curve fit the goodness of fit is indicated by R^2 . For testing differences between the

271 latency of tone-evoked spikes (Fig. 4D and 6D) we analysed the highest five SPLs because: 1. the higher n
272 numbers at these louder SPLs provided more rigorous power, 2. The latencies at these higher SPLs reached
273 a plateau and therefore did not markedly change.

274 To measure the latency to transduction current onset we plotted a linear fit to the current trace 150 ms after
275 tone onset of the adapted transduction current. A second line was plotted between the peak transduction
276 current and tone onset. Latency was taken as the intercept between these two lines. The discrete
277 depolarisations added significantly to the noise, hence why an average of the current was taken.

278 This is the first study to measure the effects of noise exposure on the locust's auditory system. Thus, we had
279 no *a priori* effect size for power calculations but we will be able to use the effect sizes reported here for power
280 calculations for future studies using the locust ear as a model for hearing loss.

281

282 **Results**

283 *Biomechanics of the tympanum*

284 We first focused our analyses on *in vivo* measures of hearing impairment after auditory overexposure. Noise-
285 exposed locusts were exposed to a 126 dB SPL 3 kHz tone for 24 hours, whereas control locusts were held
286 in identical conditions but under a silent speaker. For an *in vivo* measure of hearing impairment, we exploited
287 the accessible nature of the locust ear to measure *in vivo* tone-evoked vibrations from the external surface
288 of the tympanum, directly opposite where Group III auditory neurons are attached on the inside of the
289 tympanum. Group III auditory neurons form the majority ~46 of ~80 neurons in the Müller's organ and are
290 broadly tuned to 3 kHz (Jacobs et al., 1999; Warren and Matheson, 2018). For multiple auditory systems
291 across phyla (including humans) the health of the auditory receptor cells can be surveyed from the sounds
292 produced by mechanical vibrations of the tympanum (Kemp, 2002). Therefore, we measured the
293 displacement and mechanical gain of the tympanum. Mechanical gain is the amplitude of vibrations as a
294 function of sound amplitude. The displacement of the tympanum and its mechanical gain was increased
295 across Sound Pressure Levels (SPLs) from 50-100 dB SPL for noise-exposed locusts (Fig. 1Ai, 1Aii;
296 Displacement of tympanum: Linear Mixed Effects Model (LMEM) $t_{(86.0)}4.829$, $p < 0.0001$, effect size

297 $d=0.75896$; Mechanical gain: LMEM $t_{(79.18)}=-3.432$, $p=0.0009$, effect size $d=3.44854$; Control: $n=7$, $N=7$;
298 Noise-exposed: $n=8$, $N=8$).

299 In order to quantitatively record tone-evoked currents and spikes from individual auditory neurons the ear
300 was excised from the locust, and the Müller's organ was immersed in saline. This is necessary to gain access
301 to, image and record from individual auditory neurons through whole-cell patch-clamp intracellular recordings
302 (Warren & Matheson, 2018). We quantified the reduction in tone-evoked tympanal vibrations when the
303 tympanum is backed by water – as opposed to its tracheal air backing when *in vivo* (Fig. 1Bi, Bii). We found
304 that vibrations of the tympanum were 100 times lower when the tympanum was backed by saline or, put
305 another way; we required a tone 40 dB louder to move the tympanum by the same amount when backed by
306 saline as opposed to air (Fig. 1C).

307 *In vivo electrophysiology*

308 Next, we investigated the effect of noise-exposure on the ability of auditory neurons to produce sound-evoked
309 spikes. To accomplish this, we recorded tone-evoked nerve potentials from the auditory nerve (nerve six)
310 with hook electrodes in an *in vivo* preparation that left the first abdominal segment, with its bilateral ears,
311 intact (Fig. 2A). The nerve potentials are a read out of the population activity of Müller's organ auditory
312 neurons. The majority of the auditory neurons are broadly tuned to 3 kHz (Jacobs et al., 1999), so we used
313 a 3 kHz tone to elicit nerve potentials which were recorded as multiphasic extracellular potentials with a short
314 delay (Fig. 2Bi, ii). An increased sound amplitude elicited an increase in the nerve potentials (Fig. 2Ci, ii, iii).

315 Noise-exposed locusts replicated other hearing models with delayed spike generation in their auditory nerves
316 compared to control locust ears (Fig. 2D; LMEM $t_{(213.9)}=0.457$ $p=0.001$, effect size $d=0.666374$). Both control
317 and noise-exposed locusts' spike latency were reduced at higher sound amplitudes. Tone-evoked nerve
318 potentials, above 50 μV in amplitude, were positively correlated with sound amplitude which was well fitted
319 with a Boltzmann equation (Fig. 2E, solid lines; Control $R^2=0.962$; Noise-exposed $R^2=0.997$) but noise-
320 exposure had no significant decrease on the number of nerve potentials (LMEM $t_{(27.27)}=0.690$, $p=0.496$). We
321 determined threshold responses to 3 kHz tones (Fig. 2E, inset), which was not different between control and
322 noise-exposed locusts (Wlixon test $W=43$, $p=0.147$). We also measured the peak amplitude of the nerve
323 potentials (Fig. 2Ciii, double-headed arrows), which is the summated response of multiple spikes, typically
324 elicited at tone onset. The peak amplitude was well fitted with a Boltzmann relationship (Control $R^2=0.973$;

325 Noise-exposed $R^2=0.986$), and the peak amplitude of noise-exposed locusts was below that of their control
326 counterparts, but only for higher SPLs (Fig. 2F; LMEM: Treatment x SPL interaction, $t_{(649.0)}=10.00$ $p<0.0001$,
327 effect size $d=1.138042$).

328 *Auditory neuron morphology, electrical properties and transduction current*

329 We measured auditory neuron morphology, characterised their electrical properties and measured their
330 sound-elicited currents through whole-cell patch-clamp recordings from individual neurons from excised ears.
331 Group III neurons in Müller's organ (Fig. 3A,B,C) have a long ~ 100 μm dendrite whose length and diameter
332 was not different between control and noise-exposed locusts (Fig. 4C, Table 1). In addition, there were no
333 large differences in the membrane potential, membrane resistance and capacitance between noise-exposed
334 and control auditory neurons (Table 1).

335 We isolated and optimised the transduction current at the distal ciliated end of the auditory neuron using
336 pharmacology, voltage protocols and the optimal sound stimulus (as detailed in Fig. 3). We recorded smaller
337 discrete depolarisations in the auditory neurons of noise-exposed locust auditory neurons compared to
338 control (Fig. 3D, 3E; LM $t_{(142)}=6.524$, $p<0.0001$, effect size $d=1.087299$). Discrete depolarisations are
339 assumed to be transient stochastic opening of mechanotransduction ion channels shown both in insects (Hill,
340 1983b; Warren & Matheson, 2018) and vertebrate auditory receptors (Beurg et al., 2015; Pan et al., 2013).
341 There was a significant delay in the generation of the transduction current (Fig. 3F) in noise-exposed locusts
342 compared to their control counterparts at the maximal sound amplitude of 110 dB SPL (Fig. 3G) and across
343 sound amplitudes (Fig. 3H; LMEM $t_{(109.38)}=2.225$, $p=0.0281$, effect size $d=0.54342$). The transduction current
344 increased with an increased sound amplitude. This dependence was well fitted with a Boltzmann equation
345 (Control $R^2=0.990$, Noise-exposed $R^2=0.996$) with a clear reduction in the amplitude of the transduction
346 current for noise-exposed locust auditory neurons (Fig. 3I; LMEM $t_{(138.93)}=-13.92$, $p<0.0001$, effect size
347 $d=0.69729$). The largest difference was at their maximal transduction currents which were 146 ± 45 pA and
348 78 ± 25 pA for control and noise-exposed locusts respectively (Fig. 3J).

349 *Tone-evoked dendritic spikes*

350 The transduction potential depolarises the cilium and adjacent distal dendrite of the auditory neuron, and if
351 large enough, triggers a small dendritic spike that travels to the soma to trigger a larger axonal spike in the
352 axon hillock (Warren & Matheson, 2018). Due to its morphology the assumed dendritic spike initiation site is

353 the dendrite dilation that sits $\sim 5 \mu\text{m}$ below the cilium (Fig. 3C). To measure changes in tone-evoked dendritic
354 spikes we used whole-cell patch-clamp recordings in current clamp mode. In the absence of sound
355 stimulation spontaneous spikes were recorded which tended to be lower in noise-exposed auditory neurons
356 (Control 5.8 ± 0.9 spikes per 0.5 s, $n=15$; Noise-exposed 3.4 ± 0.7 spikes per 0.5 s, $n=13$; LM $t_{(25,0)}=7.047$,
357 $p<0.0001$, Effect size $d=0.667$). The number of tone-evoked spikes increased for higher SPLs (Fig. 4A; LMEM
358 $t_{(333,0)}=7.070$, $p<0.0001$). In response to a >60 dB SPL 3 kHz tone, tone-evoked spikes were triggered which
359 closely followed a Boltzmann relationship with sound amplitude (Fig. 4B; Control: $R^2=0.965$; Noise-exposed:
360 $R^2=0.992$). The number of tone-evoked spikes tended to be (but was not significantly) less for noise-exposed
361 auditory neurons (Fig. 4B; LMEM $t_{(169,38)}=0.975$, $p=0.3309$). The latency to first spike for all neuron types
362 decreased for increased SPLs (Fig. 4C, D). The time to first spike was delayed for noise-exposed auditory
363 neurons when compared to control auditory neurons across SPLs (LM $t_{(122)}=7.154$, $p<0.0001$, effect size
364 $d=1.30566$). We measured the width of spikes at two heights (Fig. 4C) to measure possible changes in both
365 the smaller dendritic spikes and the larger axonal spikes which they trigger. To measure axonal spike width
366 we measured at half-height (Fig. 4C, Axonal spike half-width). To infer a measure of dendritic spike width we
367 measured at half of the height of the dendritic spike (Fig. 4C, Dendritic spike half-width) The height of the
368 dendritic spike was determined by taking the start of the maximum acceleration of the spike's depolarisation
369 as the dendritic spike height. The axonal and dendritic spike width was not different between noise-exposed
370 and control locusts (Control axonal spike width 0.81 ± 0.24 , $n=15$; Noise-exposed axonal spike width $0.74 \pm$
371 0.16 , $n=12$; LM $t_{(25,0)}=0.53$ $p=0.601$) (Control dendritic spike width 1.48 ± 0.44 , $n=9$; Noise-exposed dendritic
372 spike width 1.37 ± 0.23 , $n=8$; LM $t_{(15,0)}=0.641$, $p=0.531$). For each auditory neuron we measured the tone-
373 elicited potential that produced an increase in the number of spikes above the background spontaneous spike
374 rate – the dendritic spike threshold (dotted line Fig. 4Aii). The dendritic spike threshold was similar for control
375 and noise-exposed locust auditory neurons (Control dendritic spike threshold 67.1 ± 5.1 mV, $n=14$; Noise-
376 exposed dendritic spike threshold 68.9 ± 5.9 mV, $n=12$, LM $t_{(24,0)}=0.822$, $p=0.419$).

377

378 *Current-injected axonal spikes*

379 Auditory neurons of Orthopteran's have two spike types: a dendritic spike that propagates to the soma and
380 axonal spikes that are elicited by dendritic spikes and carry auditory information to the central nervous
381 system. Next, we focused our analyses on axonal spikes to test if changes in axonal spikes contribute to

382 auditory deficits after noise exposure. To elicit axonal spikes (with their presumed spike initiation site in the
383 axon hillock) current was injected into the soma through the patch electrode (Fig. 5A). Current injected into
384 either control or noise-exposed auditory neurons resulted in the generation of axonal spikes (Fig. 5Ai, ii, iii).
385 The spike rate varied as a power law of the injected current, with no difference between control and noise-
386 exposed auditory neurons (Fig. 5B; (LMEM $t_{(28,38)}=-0.054$, $p=0.9575$). The spike latency (Fig. 5C) decreased
387 for increasing current injections (Fig. 5D) and there was no meaningful difference in latency between control
388 and noise-exposed auditory neurons (Fig. 5D; LMEM $t_{(58,24)}=-1.273$, $p=0.208$).

389 *Streptomycin block of the mechanotransduction channels mimics noise-exposure*

390 We showed a decreased amplitude of spontaneous openings (discrete depolarisations) of the
391 mechanotransduction ion channels (Fig. 3E) and decreased tone-evoked transduction current after noise
392 exposure (Fig. 3J). To mimic this effect we used the known mechanotransduction ion channel blocker
393 dihydrostreptomycin to half block the mechanotransduction channels of control locusts not exposed to noise
394 (Warren and Matheson, 2018). Blocking of the mechanotransduction ion channels had no effect on the ability
395 to elicit spikes through current injection into the soma (Fig. 6A; LMEM $t_{(39,38)}=0.087$, $p=0.9313$) or their latency
396 (Fig. 6B; Control vs Noise-exposed LMEM $t_{(76,33)}=-1.189$, $p=0.237$; Control vs Streptomycin LMEM
397 $t_{(84,42)}=0.646$, $p=0.520$; Noise-exposed vs Streptomycin LMEM $t_{(84,5)}=-1.838$, $p=0.0696$), thus mimicking
398 auditory neurons from noise-exposed ears. The application of 50 μM streptomycin reduced the tone-evoked
399 spikes compared to control ((LMEM $t_{(241,76)}=-2.970$, $p=0.0033$), which was similar to noise-exposed auditory
400 neurons only for higher SPLs >85 dB SPL (Fig. 6C). The spontaneous spike rate - which led to stark
401 differences in the number of tone-evoked spikes at lower SPLs - was significantly lower in the presence of
402 50 μM streptomycin compared to control locust auditory neurons (Fig. 6C) and tended to be lower compared
403 to noise-exposed auditory neurons. The latency of tone-evoked spikes was increased in the streptomycin
404 treated auditory neurons, compared to controls (LM $t_{(172)}=7.241$, $p<0.0001$), but remained similar to the noise-
405 exposed locusts (Fig. 6D; (LM $t_{(142)}=1.816$, $p=0.0711$)).

406 *Transcriptome analysis reveals no change in expression of the mechanotransduction ion channel candidates*

407 The reduction in the transduction current could be explained by a reduction in expression of the
408 mechanotransduction ion channels. To measure expression of the putative transduction ion channels we
409 extracted RNA from 320 Müller's organs from 160 control and noise-exposed locusts (two ears per locust).

410 We analysed the RNA reads (sequenced by Beijing Genomics Institute) and quantified expression levels for
411 the three genes that compose the two mechanotransduction ion channel candidates in insects: *nompC*,
412 *nanchung* and *inactive* (*nanchung* and *inactive* together code a single Nanchung-Inactive ion channel) and
413 two housekeeping genes *actin* and *GAPDH*. We found no change in the expression level of any three of the
414 genes that code the candidate mechanotransduction ion channels (Fig. 7).

415

416 Discussion

417 Although most noise-induced hearing loss begins with the overstimulation of primary auditory receptors we
418 lack a characterisation of their electrical properties and electrical currents after acoustic overexposure for any
419 animal ear. We used the physiologically accessible tympanal ear of the locust to quantitatively characterise
420 changes in auditory neurons after noise exposure.

421 *Biomechanical responses of the tympanum*

422 Sound-induced movements of human tympani, and the noises they produce (otoacoustic emissions), are
423 routinely used to assay the health of the auditory receptors buried deep within the inner ear. Thus, the
424 tympanum is not a simple passive receiver but can be influenced by the active force-producing mechanical
425 properties of the primary auditory receptors themselves. Although first discovered in humans (Kemp, 1978),
426 this principle extends to the ears of reptiles (Manley et al., 2001), amphibians (Long et al., 1996), birds
427 (Taschenberger & Manley, 1997) and multiple insects (Mhatre & Robert, 2013; Gopfert & Robert, 2003;
428 Gopfert & Robert, 2001). We found that the tympani of noise-exposed locust ears vibrate ~ten times higher
429 than controls across sound levels from 50-100 dB SPL. This drastic increase in compliance has three
430 probable explanations. 1. Disruption of a possible active force-producing process intrinsic to the auditory
431 neurons themselves, (Möckel et al., 2007) 2. Disruption of cytoskeletal components in the cells of Müller's
432 organ. 3. Fatigue of a muscle that could act like the middle ear muscle of humans that contracts to protect
433 the ear against loud damaging noise. Changes in the mechanics of the locust ear will, in turn, lead to changes
434 in the ability of the auditory neurons to transduce these mechanical movements into action potentials. Thus,
435 we next measured tone-evoked action potentials that are carried along the auditory nerve.

436 *In vivo electrophysiological responses of the auditory nerve*

437 The health of an auditory system – its ability to transduce sound into electrical signals - has been assayed
438 from the summated electrical potentials of the auditory nerve or auditory processing areas in the brain. After
439 acoustic overstimulation there is an increase in the auditory threshold (Coyat, et al., 2018; Christie & Eberl,
440 2014; Housley et al., 2013; Pilati et al., 2012; Telang et al., 2010; Sendowski et al., 2004; Ma et al., 1995;
441 Dolan & Mills, 1989; Pettigrew et al., 1984; Van Heusden & Smoorenburg, 1981) and a decrease in the
442 sound-evoked compound action potential amplitude (Christie & Eberl, 2014; Sendowski et al., 2004; Wang
443 et al., 1992; Dolan & Mills, 1989; Pettigrew et al., 1984; Van Heusden & Smoorenburg, 1981). In the locust
444 we found, firstly, that the linear displacement of the tympanum is converted into a nonlinear sigmoidal
445 electrical response of the tympanal nerve. This is presumably due to the nonlinear filter properties inherent
446 in the mechano-electrical gating of transduction ion channels (Hummel et al., 2016). In the auditory nerve we
447 found, that the number of sound-elicited nerve potentials, was mildly decreased and their peak response,
448 which represents spike synchrony, was strongly decreased after noise-exposure. The latency to first spike
449 was significantly increased in noise-exposed locusts compared to controls which reflects increased latencies
450 measured in other noise-exposed auditory systems (Christie & Eberl, 2014; Sendowski et al., 2004; Pettigrew
451 et al., 1984; Van Heusden & Smoorenburg, 1981). A likely cause of increased latencies after noise exposure
452 is due to an increased auditory threshold. Likewise, a probable cause of a decrease in spike synchrony, or
453 peak response, is a more variable latency. Is it not known what changes take place in the auditory receptors
454 to decrease the synchrony of nerve responses and increase spike latency. To pinpoint noise-induced initial
455 changes we performed whole-cell patch-clamp recordings from primary auditory neurons.

456 *Physiological basis of a decrease in the transduction current*

457 The electrical properties of the auditory neurons such as their membrane resistance, resting membrane
458 potential and capacitance was not affected by noise exposure, although the power of our analyses was limited
459 by our sample size. Next, we analysed changes in the spontaneous and sound-evoked openings of the
460 transduction ion channels (Hill, 1983a; Warren & Matheson, 2018). There was a significant reduction in the
461 magnitude of sound-evoked transduction current and an increase in the latency to elicit the transduction
462 current. We tested if potential noise-induced changes in both, the dendritic, and axonal spike generating
463 machinery resulted in fewer sound-evoked spikes but found no difference in the threshold, latency or spike
464 width between noise-exposed and control auditory neurons. The decreased tone-evoked spikes are
465 presumably a direct consequence of the reduced transduction current. The decreased transduction current

466 measured here have multiple explanations: 1 the mechanical attachment of the auditory neurons to the
467 tympanum - and the sound-induced force delivered to them - has weakened; 2 the number of transduction
468 channels is reduced; 3 the electrochemical driving force for the ions passing through the transduction
469 channels is decreased. Ciliated auditory receptors across animals function with common biophysical
470 principles (Albert et al., 2007; Howard & Hudspeth, 1988), share striking genetic homology (Wang et al.,
471 2002) and (most probably) evolved from the same ancestral auditory receptor (Fritzsche & Beisel, 2004). Thus,
472 we address each of these three explanations in a comparative context with other auditory systems across
473 the animal kingdom.

474 *Explanation 1: a decrease in the sound-induced force.* The transduction current in noise-exposed auditory
475 neurons is reduced by half despite a ten-fold increase in sound-evoked tympanal displacements. The
476 increased movement of the locust tympanum mirrors a likely increase in compliance of the human tympanum
477 measured in soldiers exposed to impulse noise (Job et al., 2016). In the locust ear there must be a drastic
478 decrease in mechanical coupling between the tympanum and the auditory neuron cilia where these sound-
479 induced forces open transduction ion channels, otherwise we should expect an increase of the transduction
480 current after noise exposure. Despite this, the maximal transduction current asymptotes for sound amplitudes
481 approaching 110 dB SPL (Fig. 3I) suggesting that all the transduction channels are opened at these higher
482 sound levels. All together it seems unlikely that a reduction in the sound-induced force is the main cause of
483 the decreased transduction current.

484 *Explanation 2: a decrease in the transduction channel number* The second explanation is particularly hard to
485 unequivocally test because the protein/s that form/s the transduction channel have, controversially, not been
486 identified in insects – or indeed any animal ear (although in mammals, it seems, they are getting close (Qiu
487 & Müller, 2018)). We showed no change in expression of the three genes that compose the two putative
488 candidate mechanotransduction ion channels. Providing that either Nanchung-Inactive or NompC are the
489 transduction channel, the decrease in the transduction current is probably due to a decreased
490 electrochemical potential in the receptor lymph cavity that bathes extracellular surface of the, still elusive,
491 mechanotransduction ion channel.

492 *Explanation 3: a decrease in the electrochemical driving force.* We have shown no large reduction in the
493 intracellular potential of the auditory neurons, despite a large decrease in the transduction current. Thus, if a

494 decrease in electrochemical gradient causes a decreased transduction current, it must result in a decrease
495 in the extracellular electrochemical potential maintained in a specialised receptor lymph cavity that bathes the
496 external surface of the transduction channels. This could result from damage in the supporting cells that
497 pump ions. Indeed, in the fruit fly, knocked down expression of the sodium pump (Na^+/K^+ ATPase) in the
498 supporting scolopale cells that enclose the receptor lymph result in deafness and anatomical abnormalities
499 in the receptor lymph space and sensitisation to acoustic trauma (Christie & Eberl, 2014; Roy et al., 2013). A
500 similar result is found in mammals where the supporting cells (in the stria vasculairs) are oxidatively damaged
501 after noise exposure (Shi et al., 2015) and there is also a concurrent decrease in the endocochlear potential
502 (Hirose & Liberman, 2003) and normal concentrations of potassium and calcium ions (Li et al., 1997; Ma et
503 al., 1995; Vassout, 1984). It is presumably the ATP-hungry process of maintaining high electrochemical
504 gradients, through transmembrane Na^+/K^+ pumps, which makes the supporting cells a vulnerable target of
505 noise-exposure across animal phyla. This reduction in the transduction current leads to less spontaneous
506 and sound-evoked spikes which reduces the metabolic demands for these processes. Thus, this change
507 may, in fact, serve as a protective mechanism by sparing further metabolically demanding processes in
508 auditory receptors.

509 *Conclusion*

510 This study presented here is the first systematic assessment of changes in primary auditory receptors in any
511 animal after noise-exposure. The electrophysiological properties, dendritic and axonal spike properties and
512 expression of putative mechanotransduction ion channels of the auditory neurons were unchanged –
513 demonstrating the resilience of auditory neurons in the face of a demanding acoustic insult. These findings
514 mirror recent work on mammals that show an increase in hearing thresholds but without any loss of their
515 primary auditory receptors (Kujawa and Liberman, 2009; Lin et al., 2011). Thus, a shared feature of auditory
516 receptors – be it hair cells of mammals or primary auditory neurons of insects - is the incredible amount of
517 resilience – possibly reflecting the evolutionary importance and survival value of maintaining sensitive
518 hearing.

519 **Author contributions**

520 BW conceived the idea for the paper, collected and analysed the patch-clamp electrophysiological data,
521 composed Figures 3-6 and wrote the paper. GF collected all data for the *in vivo* hook electrode recordings,

522 analysed the data and composed Figure 1 and performed all statistical analyses. EK collected and analysed
523 the mechanical laser Doppler data and composed Figure 2. AF analysed and interpreted the transcriptome
524 data and composed Figure 7. GF, JCMW, EK and AF helped refine Figures, write the paper and interpret
525 data.

526

527 **References**

- 528 Albert JT, Nadrowski B, Göpfert, MC (2007) Mechanical Signatures of Transducer Gating in the
529 *Drosophila* Ear. *Curr Biol* 17: 1000-1006. DOI:<https://doi.org/10.1016/j.cub.2007.05.004>
- 530 Albert JT, Kozlov AS (2016) Comparative Aspects of Hearing in Vertebrates and Insects with Antennal
531 Ears. *Curr Biol* 26: R1050-R1061. DOI:<https://doi.org/10.1016/j.cub.2016.09.017>
- 532 Bates D, Mächler M, Bolker B, Walker S (2015) Fitting Linear Mixed-Effects Models Using lme4. *J Stat*
533 *Softw* 67:1-48. DOI:10.18637/jss.v067.i01
- 534 Beurg M, Xiong W, Zhao B, Müller U, Fettilplace R (2015) Subunit determination of the conductance of
535 hair-cell mechanotransducer channels. *Proc Natl Acad Sci U S A* 112:1589-1594.
536 DOI:10.1073/pnas.1420906112
- 537 Böttger EC, Schacht J. (2013). The mitochondrion: A perpetrator of acquired hearing loss. *Hearing*
538 *Research* 303:12-19. DOI:<https://doi.org/10.1016/j.heares.2013.01.006>
- 539 Christie KW, Eberl DF (2014) Noise-Induced Hearing Loss: New Animal Models. *Curr Opin Otolaryngol*
540 *Head and Neck surg* 22:374-383. DOI:10.1097/MOO.0000000000000086
- 541 Christie KW, Sivan-Loukianova E, Smith WC, Aldrich BT, Schon MA, Roy M, Lear BC, Eberl DF (2013)
542 Physiological, anatomical, and behavioral changes after acoustic trauma in *Drosophila*
543 *melanogaster*. *Proc Natl Acad Sci U S A* 110:15449-15454. DOI:10.1073/pnas.1307294110
- 544 Cody AR, Russell IJ (1985) Outer hair cells in the mammalian cochlea and noise-induced hearing loss.
545 *Nature* 315:662. DOI:10.1038/315662a0
- 546 Coomber B, Berger JI, Kowalkowski VL, Shackleton TM, Palmer AR, Wallace MN (2014) Neural changes
547 accompanying tinnitus following unilateral acoustic trauma in the guinea pig. *Eur J Neurosci*
548 40:2427-2441. DOI:10.1111/ejn.12580

- 549 Coyat C, Cazevielle C, Baudoux V, Larroze-Chicot P, Caumes B, Gonzalez-Gonzalez S (2018)
550 Morphological consequences of acoustic trauma on cochlear hair cells and the auditory nerve. *Int*
551 *J Neurosci* 129:580-587. DOI:10.1080/00207454.2018.1552693
- 552 Dolan TG, Mills JH (1989) Recoveries of whole-nerve AP thresholds, amplitudes and tuning curves in
553 gerbils following noise exposure. *Hearing Research* 37:193-201. DOI:https://doi.org/10.1016/0378-
554 5955(89)90022-1
- 555 Fischel-Ghodsian N, Kopke RD, Ge X (2004) Mitochondrial dysfunction in hearing loss. *Mitochondrion*
556 4:675-694. DOI:https://doi.org/10.1016/j.mito.2004.07.040
- 557 French AS (2012) Transcriptome walking: a laboratory-oriented GUI-based approach to mRNA
558 identification from deep-sequenced data. *BMC Res Notes* 5:673. DOI:10.1186/1756-0500-5-673
- 559 Fritzschn B, Beisel KW (2004) Keeping sensory cells and evolving neurons to connect them to the brain:
560 molecular conservation and novelties in vertebrate ear development. *Brain Behav Evol* 64:182-
561 197. DOI:10.1159/000079746
- 562 Furnam AC, Kujawa SG, Liberman MC (2013) Noise-induced cochlear neuropathy is selective for fibres
563 with low spontaneous rates. *J Physiol* 110:577-586. DOI: https://doi.org/10.1152/jn.00164.2013
- 564 Gillespie PG, Walker RG (2001) Molecular basis of mechanosensory transduction. *Nature* 413:194-202.
565 DOI:10.1038/35093011
- 566 Göpfert MC, Robert D (2001) Active auditory mechanics in mosquitoes. *Proc Roy Soc Lond B* 268::333-
567 339. DOI:10.1098/rspb.2000.1376
- 568 Göpfert MC, Robert D (2003) Motion generation by *Drosophila* mechanosensory neurons. *Proc Natl Acad*
569 *Sci U S A* 100:5514-5519. DOI:10.1073/pnas.0737564100
- 570 Henikoff S, Henikoff JG (1993) Performance evaluation of amino acid substitution matrices. *Proteins*
571 17:49-61. DOI:10.1002/prot.340170108
- 572 Hill KG (1983a) The physiology of locust auditory receptors. *J Comp Physiol* 152:475-482.
573 DOI:10.1007/BF00606437
- 574 Hill KG (1983b) The physiology of locust auditory receptors. *J Comp Physiol* 152:483-493.
575 DOI:10.1007/BF00606438

- 576 Hirose K., Liberman MC (2003) Lateral wall histopathology and endocochlear potential in the noise-
577 damaged mouse cochlea. *J Assoc Res Otolaryngol* 4:339-352. DOI:10.1007/s10162-002-3036-4
- 578 Housley GD, Morton-Jones R., Vlajkovic SM, Telang RS, Paramanathasivam V, Tadros SF, Wong AC,
579 Froud KE, Cederholm JM, Sivakumaran Y, Snguanwongchai P, Khakh BS, Cockayne DA, Thorne
580 PR, Ryan AF (2013) ATP-gated ion channels mediate adaptation to elevated sound levels. *Proc*
581 *Natl Acad Sci U S A* 110:7494-7499. DOI:10.1073/pnas.1222295110
- 582 Howard J, Hudspeth AJ (1988) Compliance of the hair bundle associated with gating of mechano-electrical
583 transduction channels in the bullfrog's saccular hair cell. *Neuro*, 1:189-199.
584 [https://doi.org/10.1016/0896-6273\(88\)90139-0](https://doi.org/10.1016/0896-6273(88)90139-0)
- 585 Hummel J, Schöneich S, Kössl M, Scherberich J, Hedwig B, Prinz S, Nowotny M (2016) Gating of
586 acoustic transducer channels is shaped by biomechanical filter processes. *J Neurosci* 36: 2377-
587 2382. DOI:10.1523/JNEUROSCI.3948-15.2016
- 588 Jacobs K, Otte B, Lakes-Harlan R (1999) Tympanal receptor cells of *Schistocerca gregaria*: Correlation of
589 soma positions and dendrite attachment sites, central projections and physiologies. *J Exp Zool*
590 283:270-285. DOI:10.1002/(sici)1097-010x(19990215)283:3<270::Aid-jez5>3.0.Co;2-c
- 591 Job A, Hamery P, De Mezzo S, Fialaire JC, Roux A, Untereiner M, Cardinale F, Michel H, Klein C,
592 Belcourt B (2016) Rifle impulse noise affects middle-ear compliance in soldiers wearing protective
593 earplugs. *Int J Audiol* 55:30-37. DOI:10.3109/14992027.2015.1070967
- 594 Kemp DT (1978) Stimulated acoustic emissions from within the human auditory system. *J Acoust Soc Am*
595 64:1386-1391. DOI:10.1121/1.382104
- 596 Kemp DT (2002) Otoacoustic emissions, their origin in cochlear function, and use. *Br Med Bull* 63:223-
597 241. DOI:10.1093/bmb/63.1.223
- 598 Kujawa SG, Liberman MC (2009) Adding insult to injury: cochlear nerve degeneration after "temporary"
599 noise-induced hearing loss. *J Neurosci* 29:14077-14085. DOI:10.1523/jneurosci.2845-09.2009
- 600 Kuznetsova A, Brockhoff PB, Christensen RHB (2017) Package: Tests in Linear Mixed Effects Models. *J*
601 *Stat Softw* 82:1-26. DOI:10.18637/jss.v082.i13
- 602 Li W, Zhao L, Jiang S, Gu R (1997) Effects of high intensity impulse noise on ionic concentrations in
603 cochlear endolymph of the guinea pig. *Chinese Medical Journal* 110:883-886.

- 604 Liberman LD, Liberman CL (2015) Dynamics of cochlear synaptopathy after acoustic overexposure. *J*
605 *Acoustl Soc Am* 16:205-219. DOI: 10.1007/s10162-015-0510-3
- 606 Lin WH, Furman AC, Kujawa SG, Liberman MC (2011) Primary neural degeneration in the Guinea Pig
607 cochlea after reversible noise-induced threshold shift. *J Assoc Res Otolaryngol* 12:605-616. DOI:
608 10.1007/s10162-011-0277-0
- 609 Long GR, Dijk PV, Wit HP (1996) Temperature dependence of spontaneous otoacoustic emissions in the
610 edible frog (*Rana esculenta*). *Hearing Research* 98:22-28. DOI:https://doi.org/10.1016/0378-
611 5955(96)00057-3
- 612 Lundström R, Johansson RS (1986) Acute impairment of the sensitivity of skin mechanoreceptive units
613 caused by vibration exposure of the hand. *Ergonomics* 29:687-698.
614 DOI:10.1080/00140138608968303
- 615 Ma YL, Gerhardt KJ, Curtis LM, Rybak LP, Whitworth C, Rarey KE (1995) Combined effects of
616 adrenalectomy and noise exposure on compound action potentials, endocochlear potentials and
617 endolymphatic potassium concentrations. *Hearing Research* 91:79-86.
618 DOI:https://doi.org/10.1016/0378-5955(95)00172-7
- 619 Manley GA, Kirk DL, Koppl C, Yates GK (2001) *In vivo* evidence for a cochlear amplifier in the hair-cell
620 bundle of lizards. *Proc Natl Acad Sci U S A* 98:2826-2831. DOI:10.1073/pnas.041604998
- 621 Marcotti W, van Netten SM, Kros CJ (2005) The aminoglycoside antibiotic dihydrostreptomycin rapidly
622 enters mouse outer hair cells through the mechano-electrical transducer channels. *J Physiol*
623 567:505-521. DOI:10.1113/jphysiol.2005.085951
- 624 Mhatre N, Robert D (2013) A tympanal insect ear exploits a critical oscillator for active amplification and
625 tuning. *Curr Biol* 23:1952-1957. DOI:10.1016/j.cub.2013.08.028
- 626 Möckel D, Seyfarth E-A, Kössl M (2007) The gerneation of DPOAEs in the locust is contingent upon the
627 sensory neurons. *J Comp Physiol A* 193:871-879. DOI: doi.org/10.1007/s00359-007-0239-5
- 628 Oldfield BP, Hill KG (1986) Functional organization of insect auditory sensilla. *J Comp Physiol A* 158:27-
629 34. DOI:10.1007/bf00614517

- 630 Pan B, Géléoc GS, Asai, Y, Horwitz GC, Kurima K, Ishikawa K, Kawahima Y, Griffith AJ, Holt JR (2013)
631 TMC1 and TMC2 Are Components of the Mechanotransduction Channel in Hair Cells of the
632 Mammalian Inner Ear. *Neuron* 79:504-515. DOI:<https://doi.org/10.1016/j.neuron.2013.06.019>
- 633 Pettigrew AM, Liberman MC, Kiang NY (1984) Click-evoked gross potentials and single-unit thresholds in
634 acoustically traumatized cats. *Ann Otol Rhinol Laryngol* 112:83-96.
635 DOI:<https://doi.org/10.1177/00034894840930S416>
- 636 Pilati N, Large C, Forsythe ID, Hamann M (2012) Acoustic over-exposure triggers burst firing in dorsal
637 cochlear nucleus fusiform cells. *Hearing Research* 283:98-106. DOI:10.1016/j.heares.2011.10.008
- 638 Pujol, R., Puel, J. L., Gervais d'Aldin, C., & Eybalin, M (1993) Pathophysiology of the glutamatergic
639 synapses in the cochlea. *Acta Otolaryngologica* 113:330-334.
640 DOI:<http://doi.org/10.3109/00016489309135819>
- 641 Qiu X, Müller U (2018) Mechanically Gated Ion Channels in Mammalian Hair Cells. *Front Cell Neurosci*
642 12:100. DOI:10.3389/fncel.2018.00100
- 643 Römer H (1976) Die Informationsverarbeitung tympanaler Rezeptorelemente von *Locusta migratoria*
644 (Arctrididae, Orthoptera). *J. Comp. Physiol.* 109:101-122. DOI: 10.1007/BF00663438
- 645 Roy M, Sivan-Loukianova E, Eberl DF (2013) Cell-type–specific roles of Na⁺/K⁺ ATPase subunits in
646 *Drosophila* auditory mechanosensation. *Proc Natl Acad Sci U S A* 110:181-186.
647 DOI:10.1073/pnas.1208866110
- 648 Salvi R, Boettcher FA (2008) Animal Models of Noise-Induced Hearing Loss. In *Sourcebook of Models for*
649 *Biomedical Research* (Editor Conn PM) (pp. 289-301). Totowa, New Jersey: Humana Press.
- 650 Salvi R, Henderson D, Hamernik RP, Parkins C (1980) VIII nerve response to click stimuli in normal and
651 pathological cochleas. *Hearing Research* 2:335-342. DOI:[https://doi.org/10.1016/0378-](https://doi.org/10.1016/0378-5955(80)90067-2)
652 [5955\(80\)90067-2](https://doi.org/10.1016/0378-5955(80)90067-2)
- 653 Sendowski I, Brailon-Cros A, Delaunay C (2004) CAP amplitude after impulse noise exposure in guinea
654 pigs. *Eur Arch Otorhinolaryngol* 261:77-81. DOI:10.1007/s00405-003-0647-2
- 655 Shi L, Guo X, Shen P, Liu L, Tao S, Li X, Song Q, Yu Z, Yin S, Wang J (2015) Noise-induced damage to
656 ribbon synapses without permanent threshold shifts in neonatal mice. *Neurosci* 304:368-377.
657 DOI:<https://doi.org/10.1016/j.neuroscience.2015.07.066>

- 658 Shi X, Nuttall AL (2003) Upregulated iNOS and oxidative damage to the cochlear stria vascularis due to
659 noise stress. *Brain Research* 967:1-10. DOI:10.1016/s0006-8993(02)04090-8
- 660 Taschenberger G, Manley GA (1997) Spontaneous otoacoustic emissions in the barn owl. *Hearing*
661 *Research* 110:61-76. DOI:[https://doi.org/10.1016/S0378-5955\(97\)00070-1](https://doi.org/10.1016/S0378-5955(97)00070-1)
- 662 Telang RS, Paramanathasivam V, Vlajkovic SM, Munoz DJB, Housley GD, Thorne PR (2010) Reduced
663 P2x(2) receptor-mediated regulation of endocochlear potential in the ageing mouse cochlea.
664 *Purinergic Signal* 6:263-272. DOI:10.1007/s11302-010-9195-6
- 665 Van Heusden E, Smoorenburg GF (1981) Eighth-nerve action potentials evoked by tone bursts in cats
666 before and after inducement of an acute noise trauma. *Hearing Research* 5:1-23. DOI:
667 [https://doi.org/10.1016/0378-5955\(81\)90024-1](https://doi.org/10.1016/0378-5955(81)90024-1)
- 668 Vassout P. 1984. Effect of pure tone on endocochlear potential and potassium ion concentration in the
669 guinea pig cochlea. *Acta Otolaryngology*, **98**(3-4), 199-203.
670 DOI:<https://doi.org/10.3109/00016488409107555>
- 671 Wagner EL, Shin JB (2019) Mechanisms of Hair Cell Damage and Repair. *Trends Neurosci* 42:414-424.
672 DOI:10.1016/j.tins.2019.03.006
- 673 Wang VY, Hassan BA, Bellen HJ, Zoghbi HY (2002) *Drosophila* atonal fully rescues the phenotype of
674 Math1 null mice: new functions evolve in new cellular contexts. *Curr Biol* 12:1611-1616. DOI:
675 [https://doi.org/10.1016/S0960-9822\(02\)01144-2](https://doi.org/10.1016/S0960-9822(02)01144-2)
- 676 Wang J, Li Q, Dong W, Chen J (1992) Effects of various noise exposures on endocochlear potentials
677 correlated with cochlear gross responses. *Hearing Research* 59:31-38.
678 DOI:[https://doi.org/10.1016/0378-5955\(92\)90099-9](https://doi.org/10.1016/0378-5955(92)90099-9)
- 679 Warren B, Matheson T (2018) The Role of the Mechanotransduction Ion Channel Candidate Nanchung-
680 Inactive in Auditory Transduction in an Insect Ear. *J Neurosci* 38:3741-3752.
681 DOI:10.1523/jneurosci.2310-17.2018
- 682 Young RW (1988) Solar radiation and age-related macular degeneration. *Surv Ophthalmol* 32:252-269.
683 DOI: [https://doi.org/10.1016/0039-6257\(88\)90174-9](https://doi.org/10.1016/0039-6257(88)90174-9)
- 684
- 685

686
687
688
689
690
691
692
693
694
695
696
697
698
699

700 **Figure captions**

701 **Figure 1** *In vivo* Doppler laser measurements of tympanal displacements shows increased displacements and gain for
702 noise-exposed locusts. **Ai.** The displacement of the tympanum was higher for noise-exposed locusts. **Aii** The gain, nm
703 displacement per Pascal, was also higher for noise-exposed locusts. **Bi.** The experimental setup for *in vivo* recording
704 from an intact ear. **Bii** Experimental setup for *ex vivo* recording with a saline-backed tympanum, necessary for
705 intracellular recordings from individual auditory neurons. **C.** Comparison of tympanal displacements in an *in vivo* and *ex*
706 *vivo* preparation backed by air and saline respectively. A 40 dB louder tone is required to move the tympanum by the
707 same amount when backed by saline (*ex vivo*) compared to air (*in vivo*).

708 **Figure 2** *In vivo* hook electrode recordings from the auditory nerve (six). Neuron schematic on left, with red circle,
709 indicates where the electrical signals were recorded – from the auditory nerve. **A.** Schematic showing the vivisection
710 and placements of the hook electrodes under the auditory nerve. **Bi.** Example recording using a 3 kHz tone at 90 dB

711 SPL **Bii** with an expanded view (of dotted box in **Bi**) to show latency to first nerve potential and the 50 μ V threshold
712 used to count nerve potentials. **C**. Nerve responses for a 0.5 s 3 kHz tone at **Ci** 30, **Cii** 70, and **Ciii** 110 dB SPL (peak
713 amplitude calculation for **F** is shown with double headed arrows). **D**. Quantification of the latency to first nerve potential
714 in response to a 3 kHz tone for control and noise-exposed locusts. Means are plotted as circles, positive standard
715 deviation is plotted as error bars. One auditory nerve from a noise-exposed locust had an extremely high spontaneous
716 spike rate and was not included in the latency analysis. **E**. Quantification of the number of tone-evoked nerve potentials
717 above 50 μ V, which increased for louder sound amplitudes. Nerve potential counts are well fitted with Boltzmann
718 equations (solid lines). Means are plotted as circles, positive standard deviation is plotted as error bars (the error bars
719 for noise-exposed means are offset, right, for figure clarity). Nerve potential counts from individual locusts are plotted
720 as thin shaded lines. One auditory nerve from a noise-exposed locust did not show any response to even the highest
721 SPLs. N.B. Two individual particularly high nerve potential counts, included in the analysis, are plotted as dotted lines on
722 the right axis. Inset are the thresholds SPLs for all recordings. **F**. The peak amplitude response of control locusts was
723 higher than noise-exposed locusts at higher SPLs. The peak response increased for higher sound amplitudes and was
724 well fitted with a Boltzmann equation (solid lines).

725

726 **Figure 3** Intracellular whole-cell patch-clamp recordings of auditory neurons, their spontaneous and tone-evoked
727 transduction ion channel activity and neuron morphology. All spontaneous and tone-evoked transduction currents
728 occur in the auditory neurons' cilium highlighted by a red circle on the neuron schematic on the left. **A**. Schematic
729 showing experimental setup for intracellular patch-clamp recordings from Müller's organ housed on the internal
730 surface of the tympanum perfused with saline. The outside of the tympanum is acoustically driven by airborne sound
731 by a speaker. **B**. Double staining of the nuclei of cells of Müller's organ (magenta, DAPI) and all auditory neurons with
732 whole nerve backfill using neurobiotin/Dylight 488 streptavidin (green). Group-III auditory neurons are highlighted by a
733 white dotted circle. **C**. A neurobiotin-streptavidin staining of two Group-III auditory neurons *in situ* reveals the dendrite
734 dilation and apical cilium. **D**. Sound stimulation, voltage-clamp and recording protocol used to maximise the
735 transduction current during intracellular patch-clamp recordings. A 3 kHz tone at 110 dB SPL (top trace) was used to
736 stimulate Group-III auditory neurons at their most sensitive frequency. The neurons were voltage-clamped to -100 mV
737 (grey trace) to increase the electrochemical driving force. The extracellular saline contained 90 nM TTX and
738 intracellular pipette solution contained 20 mM TEA to block sodium and potassium conductances and the spikes they
739 facilitate. Discrete depolarisations (arrows) and the tone-evoked transduction currents are reduced in noise-exposed
740 auditory neurons (red) compared to control (black). **E**. The amplitude of discrete depolarisations is reduced for
741 auditory neurons from noise-exposed ears. The maximum six discrete depolarisations were averaged for each locust
742 during the -100 mV voltage clamp. **F**. Example showing calculation of the latency of the tone-evoked transduction

743 current. **G.** Latency of the transduction current was delayed for noise-exposed auditory neurons at 110 dB SPL and **H.**
744 across sound intensities. **I.** The transduction current increased with louder sound amplitudes, which was well fitted
745 with a Boltzmann equation (solid lines). Mean is plotted as circles, positive standard deviation is plotted as shaded
746 area, transduction current amplitude from individual auditory neurons are plotted as thin shaded lines. (Control: n=12,
747 N=6; Noise-exposed: n=12, N=7). **J.** The maximal transduction current was significantly reduced at the maximal
748 sound intensity of 110 dB SPL.

749

750 **Figure 4** Tone-evoked spikes were recorded in current clamp mode with whole-cell patch-clamp recordings from
751 auditory neurons from control and noise-exposed locust ears. Dendritic spikes are elicited in the distal part of the
752 dendrite, with its presumed site highlighted by the red circle, left. **Ai, ii, iii.** Example recordings from control and noise-
753 exposed auditory neurons when played a 0.5 s 3 kHz tone at 65, 85 and 110 dB SPL. The grey dotted line in **Aii** indicates
754 the potential at which a dendritic spike threshold was calculated. **B.** The number of tone-evoked spikes was higher for
755 louder sound amplitudes which was well fitted by a Boltzmann equation (solid lines). Mean is plotted as circles, positive
756 standard deviation is plotted as shaded area, spike counts from individual locusts are plotted as thin shaded lines
757 (Control: n=15, N=8; noise-exposed: n=13, N=12). **C.** Example recording showing how the latency of tone-evoked spike
758 was measured and a rare isolated dendritic spike (grey) later in the same recording, which is overlaid on the larger
759 axonal spike. Dotted lines indicate where the axonal spike half-width and dendritic spike half-width were measured. **D.**
760 The latency to first spike was slower for auditory neurons from noise-exposed locusts (red) compared to controls (black)
761 across sound amplitudes. Means are plotted as circles, positive standard deviation is plotted as error bars. Grey brackets
762 with asterisk denote the recordings that were statistically tested (see Statistical Experimental design and statistical
763 analysis for justification).

764

765 **Figure 5** Axonal spikes were elicited through current injection into the auditory neuron somata of control and noise-
766 exposed locust ears. Axonal spikes are assumed to be triggered in the axon hillock, red circle left. **A** Example recordings
767 showing **Ai** spontaneous spikes and **Aii** spikes in response to 100 pA current injection and **Aiii** spikes in response to
768 300 pA current injection. **B.** The number of spikes triggered by current injection was fitted by a power law (solid lines)
769 and was not different for auditory neurons from noise exposed (red) or control locusts (black) across all current
770 injections. Means are plotted as circles, positive standard deviation is plotted as error bars (the error bars for noise-
771 exposed means are offset, right, for figure clarity). Current-elicited spike number from individual auditory neurons are
772 plotted as thin shaded lines (Control: n=12, N=9; Noise-exposed: n=11, N=10). **C** An example measurement of the
773 current-injected spike latency. **D.** Current-injected spike latency across and range of injected currents, which were not

774 different between control and noise-exposed locusts. Recordings were lost at high current injections, hence the lower n
 775 numbers at high current injections. Means are plotted as circles, positive standard deviation is plotted as error bars (One
 776 neuron from the noise-exposed group was not analysed for latency due to its high spontaneous spike rate). Grey
 777 brackets with asterisk donate the recordings that were statistically tested (see Experimental design and statistical
 778 analysis for justification).

779

780 **Figure 6** Axonal spikes at the axon hillock (red circle, top left) and dendritic spikes (red circle, bottom left) were measured
 781 in response to 50 μM streptomycin (blue triangles, left). **A.** Number of current-injected spikes for noise-exposed (red),
 782 control (black) and streptomycin-perfused (blue) auditory neurons, fitted with a power law, (solid lines) were not different
 783 between all three treatments. Means are plotted as circles, positive standard deviation is plotted as error bars, current-
 784 elicited spikes from individual auditory neurons in the presence of 50 μM streptomycin are plotted as thin blue shaded
 785 lines (Control: n=12, N=9; noise-exposed: n=11, N=10; Streptomycin perfused n=14, N=10). **B.** Latency to first current-
 786 injected spike for noise-exposed (red), control (black) and streptomycin perfused (blue) auditory neurons was not
 787 different between treatments (plotted on logarithmic axis for figure clarity). **C.** Tone-evoked spikes for noise-exposed
 788 (red), controls (black) and streptomycin perfused auditory neurons fitted with a Boltzmann equation (Streptomycin
 789 $R^2=0.990$). Mean is plotted as circles, positive standard deviation is plotted as shaded area and tone-evoked spike
 790 counts, from individual auditory neurons in the presence of 50 μM streptomycin, are plotted as thin blue lines. **D.** Tone-
 791 evoked spike latency for noise-exposed (red), controls (black) and streptomycin perfused (blue) auditory neurons
 792 (plotted on logarithmic axis for figure clarity). Grey brackets with asterisk donate the recordings that were statistically
 793 tested (see Experimental design and statistical analysis for justification).

794

795 **Figure 7** Abundance of RNA transcripts extracted from Müller's organs of control and noise-exposed locusts for house-
 796 keeping genes, *actin* and *GAPDH* and for the three genes that together code the two mechanotransduction ion channel
 797 candidates, *nanchung*, *inactive* and *nompC*. Abundance was calculated by counting all matching reads to each gene's
 798 open reading frame in the complete, groomed transcriptomes, and then normalized by the reading frame length.

799

800

801 **Table**

	Dendrite length (μm)	Dendrite diameter at midpoint (μm)	Resting potential (mV)	Membrane resistance ($\text{M}\Omega$)	Capacitance (pF)
--	-----------------------------------	---	------------------------	--	------------------

Control	114 ± 13 (n=8)	3.2 ± 0.74 (n=8)	60 ± 8 (n=11)	50 ± 47 (n=12)	25 ± 8 (n=12)
Noise-exposed	120 ± 15 (n=8)	3.1 ± 0.60 (n=8)	57 ± 5 (n=9)	54 ± 45 (n=12)	22 ± 5 (n=12)

804

805

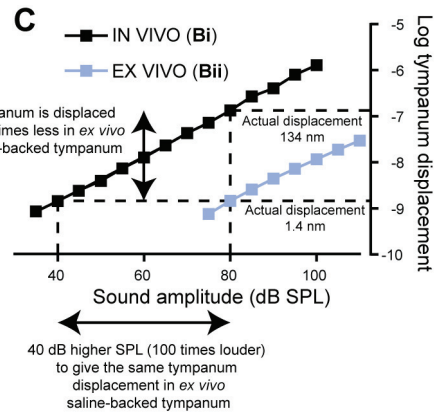
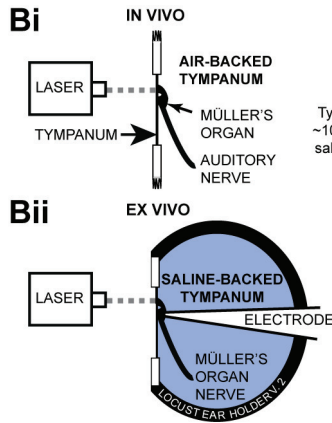
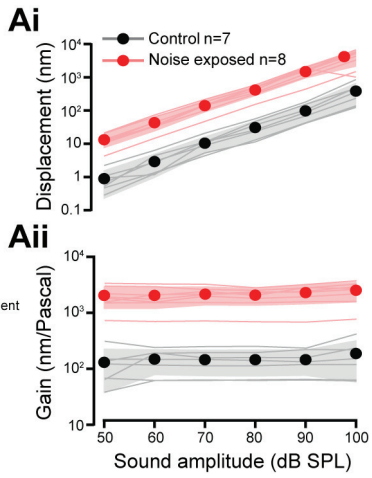
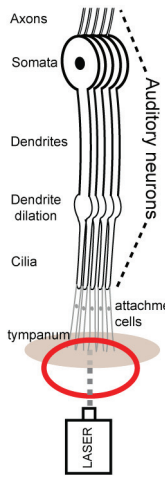
806 **Table 1.** Morphological and electrophysiological properties of auditory neurons. There were no significant differences
807 between the morphological or electrophysiological properties of noise-exposed and control auditory neurons (Linear
808 Model (LM), p= 0.464, 0.651, 0.362, 0.7826, 0.164; t= 24.51, 0.462, -0.935, -0.280, 1.441, respectively). These
809 measurements were recorded from spiking neurons with no TTX and TEA in the extracellular or intracellular saline. Only
810 neurons with a resting membrane potential at least -50mV were used to compare resting potentials.

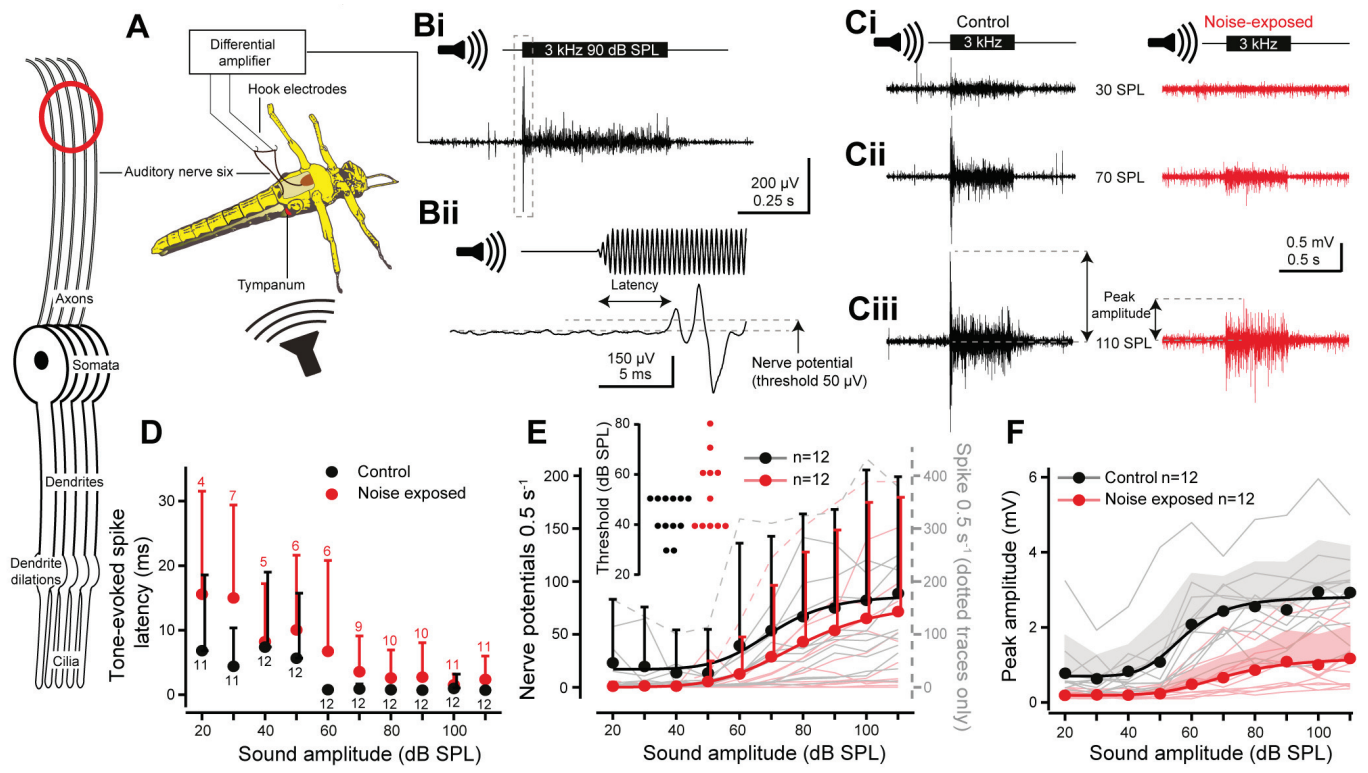
811

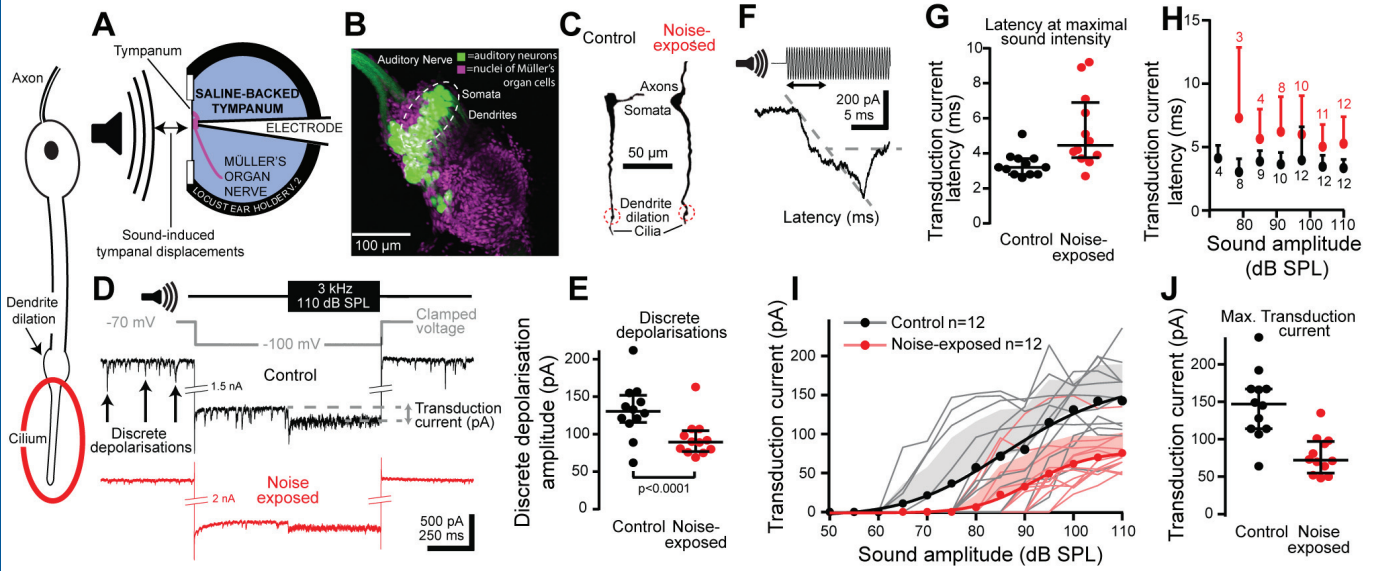
812

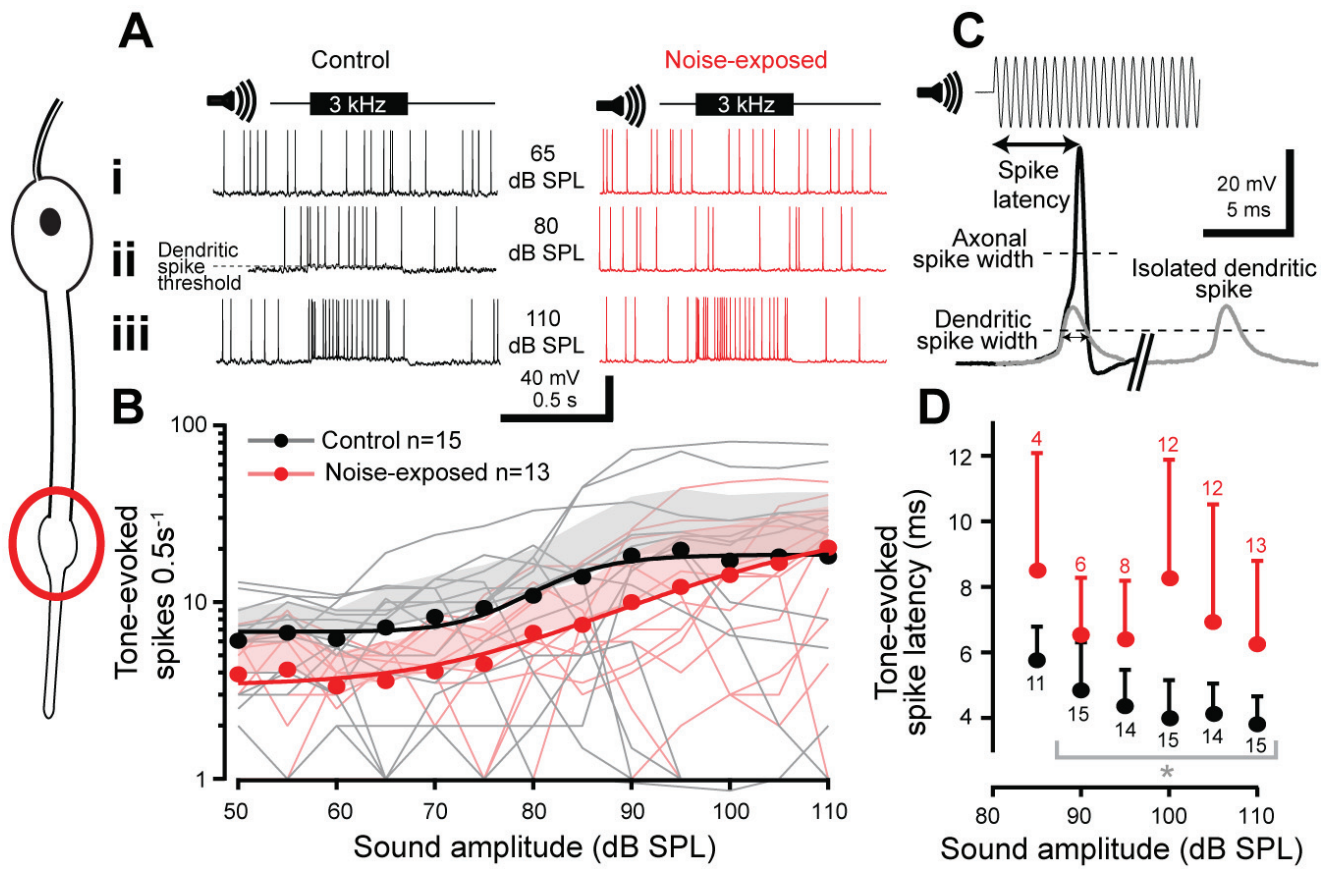
813

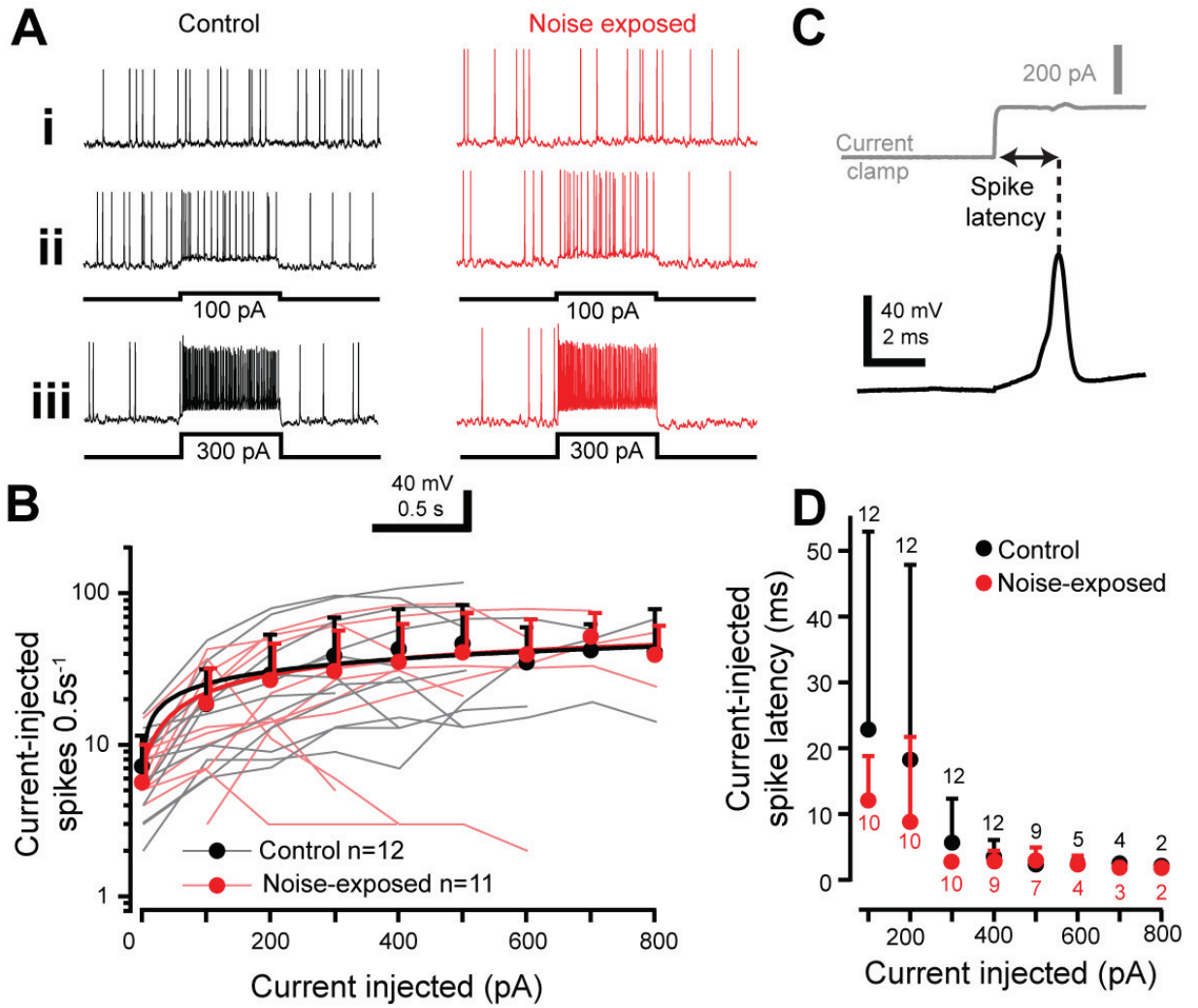
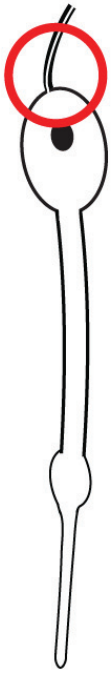
814

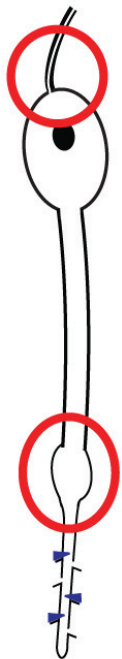












50 μ M Streptomycin half-blocks transduction channels

